Wide Operating Voltage Range Fuel Cell Battery Charger

Hernandez Botella, Juan Carlos; Mira Albert, Maria del Carmen; Sen, Gokhan; Thomsen, Ole Cornelius; Andersen, Michael A. E.

Published in:
Elektronika ir Elektrotechnika

Link to article, DOI:
10.5755/j01.eee.20.5.7107

Publication date:
2014

Document Version
Peer reviewed version

Wide Operating Voltage Range Fuel Cell Battery Charger

J. C. Hernandez[1], M. C. Mira[1], G. Sen[2], O. C. Thomsen[1], M. A. E. Andersen[1]
[1]*Department of Electrical Engineering, Technical University of Denmark, Orsteds Plads, 349. 2800 Kgs. Lyngby, Denmark*
[2]*Electrical and Electronics Engineering, University of Turkish Aeronautical Association, Bahcekapi Mah., Okul Sokak 11, 06790 Etimesgut, Ankara, Turkey*
jchbo@elektro.dtu.dk

***Abstract*—DC-DC converters for fuel cell applications require wide voltage range operation due to the unique fuel cell characteristic curve. Primary parallel isolated boost converter (PPIBC) is a boost derived topology for low voltage high current applications reaching an efficiency figure up to 98.2 %. This paper proposes a new operation mode for extending the input and output voltage range in PPIBC. The proposed solution does not modify PPIBC power stage; the converter gain is modified by short-circuiting one of the parallel connected primary windings in the topology. The change in operation mode divides by two the converter input-to-output voltage gain. This allows covering the conditions when the fuel cell stack operates in the activation region (maximum output voltage) and increases the degrees of freedom for converter optimization. The transition between operating modes is studied because represents a change in the converter steady-state conditions. A solution is proposed based on pre-calculation of the duty cycle prior to the transition.**

***Index Terms*—Isolated boost, fuel cell, battery, extended voltage range.**

I. INTRODUCTION

Due to the need for alternative energy resources, efficient power processing through power electronics circuits has been a popular academic field for the past decade. Fuel cells are one of the solutions widely adopted in uninterruptible power supplies (UPS), backup systems and electric vehicles. Fuel cells provide a clean and consistent source of energy by converting chemical energy into electrical energy. Power electronics interfacing fuel cell stacks and the rest of the power system should be designed considering some important electrical features of the fuel cell system, such as V-I characteristic curve. Among various converter topologies proposed and used in the literature, primary parallel isolated boost converter (PPIBC), derived from the conventional isolated boost converter, is a good candidate for such applications due to its simplicity and ability to handle high currents [1], [2]. However, boost type dc-dc converters have intrinsic start-up problems and limited input/output voltage range operation. Overcoming this limitation requires modification of the input inductor and employing additional circuitry [3]. In this paper an alternative solution with an extended voltage operation range is proposed based on modifying the operating mode of PPIBC. PPIBC schematic and steady-state operating waveforms under normal operating conditions are presented in Fig. 1 and Fig. 2.

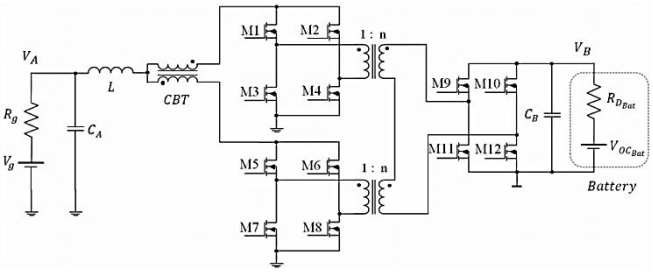

Fig. 1. Primary parallel isolated boost converter schematic.

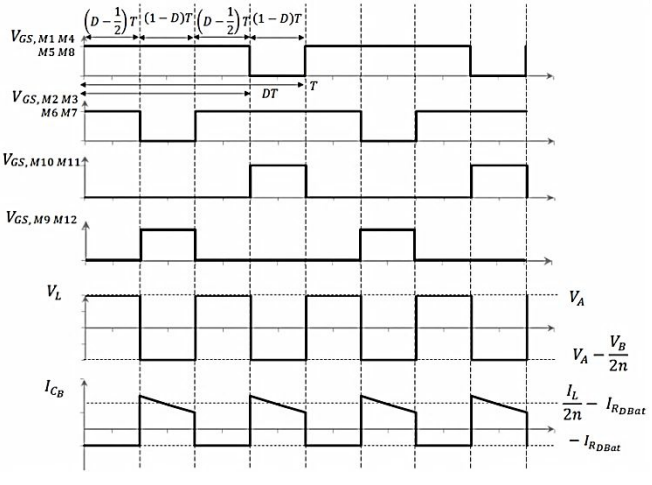

Fig. 2. Primary parallel isolated boost converter steady-state waveforms.

This topology increases the efficiency by splitting the primary current through two parallel primary stages. This approach results in reduced ac current loops, which helps reducing the power stage layout stray inductances. In addition, the secondary windings of the two transformers are connected in series, which reduces the number of turns on the secondary side for individual transformers allowing an

Manuscript received October 18, 2013; accepted December 28, 2013.

easier magnetic component design. The primary switches in each parallel stage are driven with identical gate signals. Moreover, the two stages share the input inductor as well as the input and output filters, which makes this topology a simple solution. Due to the transformer series connection on the secondary side the two currents flowing through the two primary stages are forced to be equal during the inductor discharge state. In order to balance the current between the primary stages during the inductor charging subinterval, a current balancing transformer (CBT) [4] is inserted. This component is implemented as two inversely coupled inductors that present high impedance in case of current. imbalance, keeping the current equal in each parallel stage.

In this work, PPIBC acts as a battery charging unit in a fuel cell powered electric drive train in a low speed vehicle, as shown in Fig. 3. The V-I characteristic curve of a fuel cell is a nonlinear function [5], where three different regions can be distinguished as shown in Fig. 4. Moreover, as presented in the Shepherd model [6], the battery terminal voltage strongly depends on the charging current. Due to the battery terminal voltage dependence and the voltage rise in the activation region of the fuel cell (see Fig. 4), the converter needs to be designed for a wide operating input and output voltage range. When an acceleration event occurs, the inverter current demand will reduce the battery terminal voltage; if the fuel cell stack is operating in the activation region during this event, the converter will have to present minimum input to output voltage gain.

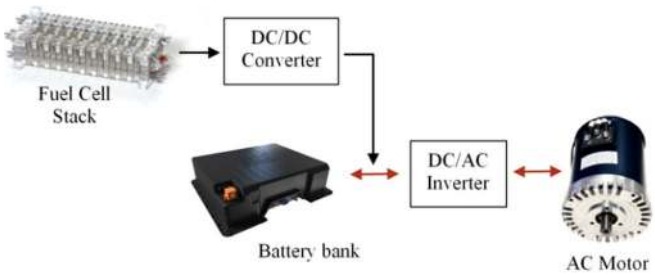

Fig. 3. Power drive train block diagram.

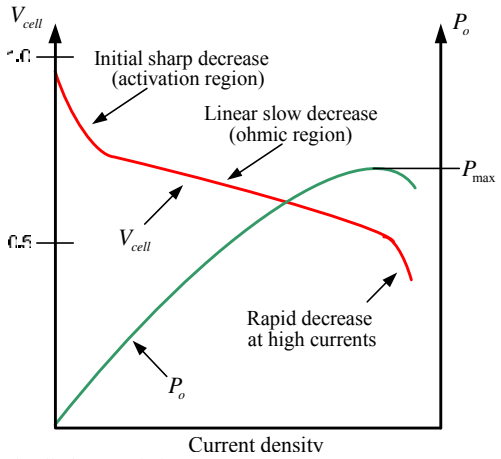

Fig. 4. Fuel cell characteristic V-I curve.

Therefore, in this application the transformer turns ratio has to be selected for the converter to operate with minimum duty cycle under these operating conditions. However, this solution will increase the converter voltage and current stresses negatively affecting the efficiency. Instead, this paper proposes a change in the converter operation mode, which increases the degrees of freedom in the design for the converter optimization.

II. Extended Operating Voltage Range

One of the disadvantages of isolated boost type dc-dc converters is the 50 % theoretical minimum duty cycle for each primary side switch, which corresponds to a "no boosting" operating point. Further decreasing the duty cycle is not possible since this will result in a practical "open circuit" situation for the input inductor. This lower limit for the switch duty cycle also puts a lower limit for the output voltage or an upper limit for the input voltage. The state of the art solution for extended voltage range in isolated boost converters has been presented in the literature [3], [7]. The solution in [3] proposes an auxiliary winding in the input inductor that will provide flyback operation to the converter, extending the operating voltage range and solving the intrinsic start-up problems in boost derived topologies. However, this is not an efficient solution in high power applications and makes the manufacturing process of the input inductor more complicated since extensive interleaving techniques will have to be adopted to increase the coupling coefficient of the flyback winding.

This work presents an efficient solution for extending the voltage range of PPIBC by implementing a new operation mode where the two upper side MOSFETs in one of the parallel stages are shut down while the lower side switches are kept in conduction mode. This new operation mode effectively reduces the equivalent converter conversion ratio by short-circuiting the primary winding in one of the primary stages, which deactivates the corresponding transformer.

As in the auxiliary flyback winding configuration, the main drawback of the proposed solution is the increased voltage stress on the primary switches during the extended operation mode. As shown in (3) the output voltage is no more divided in the series secondary windings of the two transformers. This situation will increase the requirement for the primary switch breakdown voltage, consequently increasing the device on resistance, which affects the converter efficiency. However, if the extended operation mode is only used to cover the operating conditions with minimum output voltage, the primary MOSFETs breakdown voltage requirement will not be affected.

$$V_{DS_{PPIBC}} = V_B / (2n), \quad (1)$$

$$V_{DS_{Flyback}} = V_A + V_B / (2n), \quad (2)$$

$$V_{DS_{PPIBC\_Extended}} = V_B / n. \quad (3)$$

This is an attractive solution in applications with variable output voltage, where the extended mode will be operated only under minimum output voltage.

Figure 5 shows the current path at the inductor discharge subinterval during extended operation mode of the PPIBC. As it can be observed from Fig. 5, the primary winding of the lower transformer is effectively shorted by the two low side switches, M7 and M8. The converter steady-state

waveforms are presented in Fig. 6. Figure 7 shows the converter voltage gain during extended voltage range operation; since only one transformer is active, effective voltage conversion ratio of the converter is halved as shown in (4).

$$M\left(D\right) = V_B / V_A = n / \left[2\left(1-D\right)\right]. \quad (4)$$

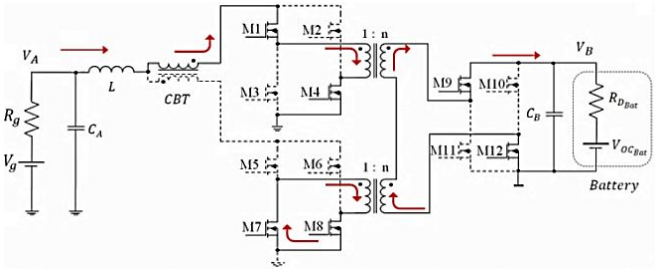

Fig. 5. PPIBC inductor discharge during extended voltage range mode.

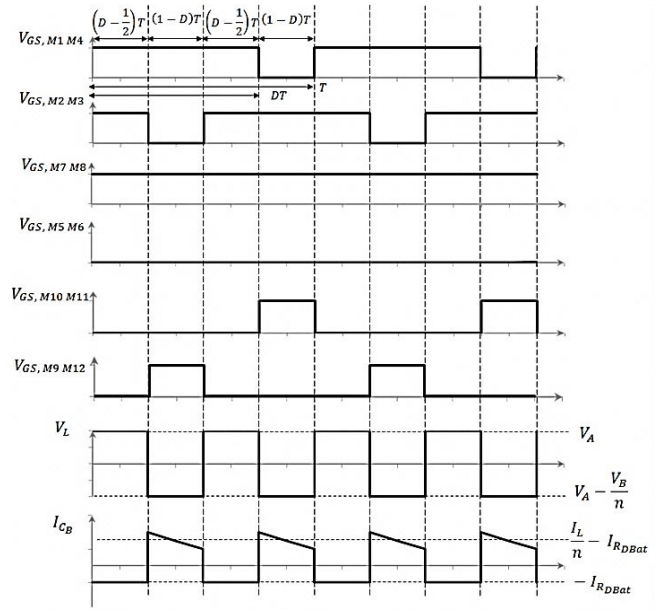

Fig. 6. PPIBC steady-state waveforms during extended voltage range operation.

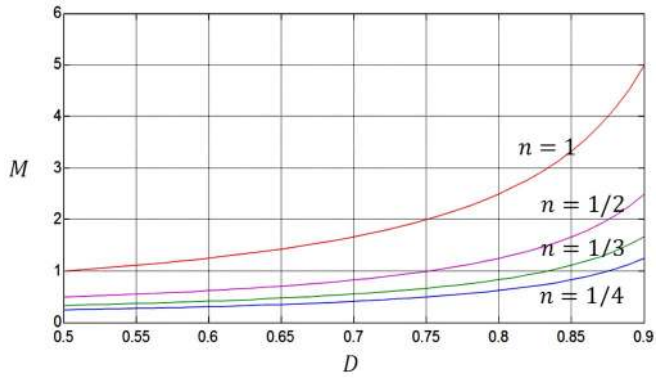

Fig. 7. Converter input to output voltage gain during extended operation mode for different transformer turns ratio.

III. Simulation of PPIBC with Extended Voltage Range Operation

The proposed solution is analysed by performing several LTspice simulations with the operating conditions shown in Table I. The transition of the converter between normal and extended operation mode needs to be investigated because the output current of the fuel cell should be stable during this event. If the operation of the converter has to be interrupted to switch from one mode to the other, a dummy load would have to be used in order to limit the output voltage of the fuel cell during the transition, and this would increase the complexity of the system.

TABLE I. PARAMETERS OF THE CONVERTER.

Source voltage	30 V
Battery terminal voltage	24 V
Transformer turn ratio	3:1
Inductor	13.5 µH
Capacitor A	40 µF
Capacitor B	120 µF
Switching frequency	50 kHz
Source output resistance	10 mΩ
Battery dynamic resistance	60 mΩ

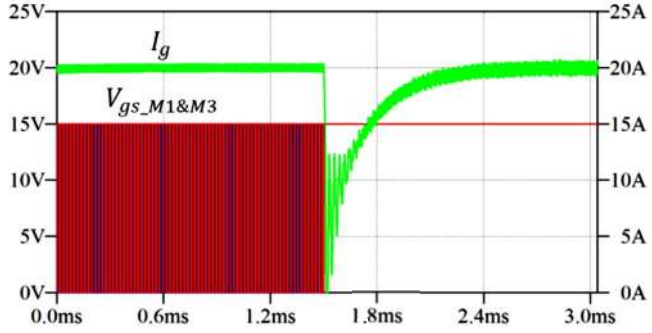

Fig. 8. Simulated transition from normal operation mode to extended operation mode. Converter input current I_g (green), M1 and M3 gate signal (red and blue).

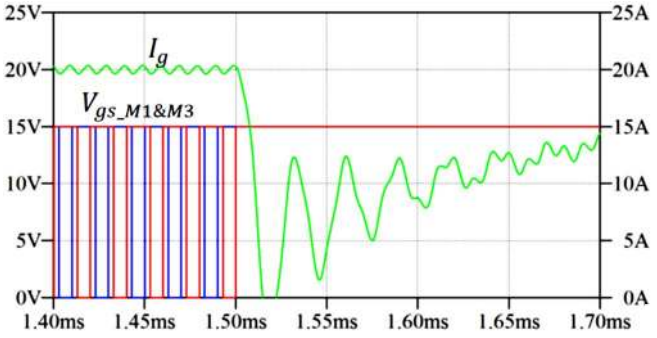

Fig. 9. Detailed enlarged area of the transition. Converter input current I_g (green), M1 and M3 gate signal (red and blue).

Figure 8 and Fig. 9 present a simulation result where the inductor current level is fixed at $20A$ during closed loop operation of the converter. It can be observed that during the transition the current deviates from the reference value until the loop is able to compensate the error. The deviation in the current during the transition is caused by the change in the converter steady-state conditions and the sensitivity of the inductor current to duty cycle perturbations, as presented in [8]. This will increase the components current stress, which will reduce the converter reliability.

IV. Transition with Pre-Calculated Steady-State Duty Cycle

The current stress during the transition time can be

reduced if a steady-state duty cycle pre-calculation is performed based on an accurately derived model of the converter. In battery loading applications, as presented in [8]–[9], the duty cycle-to-inductor current transfer function is heavily affected by the converter parasitic resistances due to the low value of the battery dynamic resistance. Circuit models taking into account parasitic resistances for both inductor charge (Fig. 10) and discharge (Fig. 11) states during extended operation mode are derived. The simplified models, shown in Fig. 12 and Fig. 13, are obtained by reflecting the secondary side impedances to the primary side and combining the two parallel full-bridge transformers to a single structure with an effective transformer ratio N_e.

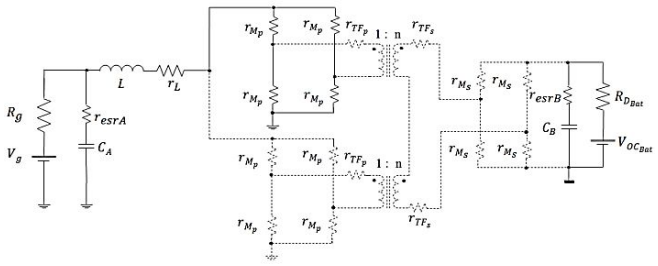

Fig. 10. PPIBC extended voltage range operation during the inductor charging subinterval.

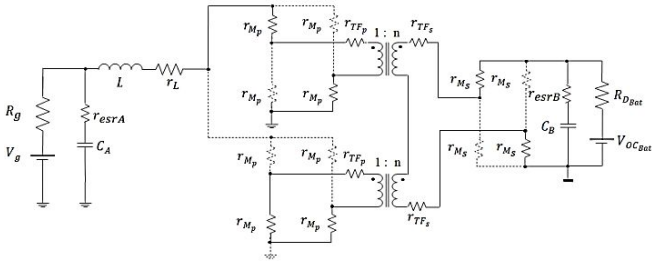

Fig. 11. PPIBC extended voltage range operation during the inductor discharging subinterval.

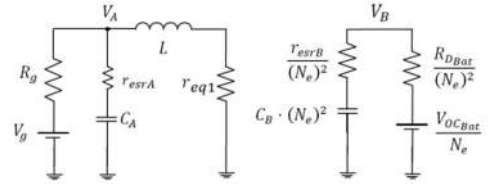

Fig. 12. PPIBC simplified equivalent circuit during the inductor charge.

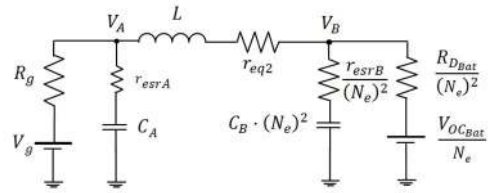

Fig. 13. PPIBC simplified equivalent circuit during the inductor discharge.

State-space equations are derived based on the two operating states of the converter [8]. The state matrixes are calculated for the inductor charging and discharging subintervals as shown in (16) and (17). The input matrix corresponding to the inductor charging subinterval is shown in (5), and the input matrix corresponding to the discharging subinterval is calculated as shown in (6):

$$B_1 = \begin{pmatrix} r_{esr_A} / \left[L\left(R_g + r_{esr_A}\right)\right] & 0 \\ 1/\left[C_A\left(R_g + r_{esr_A}\right)\right] & 0 \\ 0 & 1/\left[2C_B N_e \left(R_{D_{Bat}} + r_{esrB}\right)\right] \end{pmatrix}, \quad (5)$$

$$B_2 = \begin{pmatrix} r_{esr_A} / \left[L\left(R_g + r_{esr_A}\right)\right] & -r_{esr_A} / \left[2N_e L\left(R_{D_{Bat}} + r_{esrB}\right)\right] \\ 1/\left[C_A\left(R_g + r_{esr_A}\right)\right] & 0 \\ 0 & 1/\left[2C_B N_e \left(R_{D_{Bat}} + r_{esrB}\right)\right] \end{pmatrix}. \quad (6)$$

Equivalent transformation ratio N_e and equivalent resistances r_{eq1} and r_{eq2} are defined as shown in (7)–(9) for normal operating mode. These can be calculated in the same way for extended operating mode as shown in (10)–(12):

$$N_e = 2n, \quad (7)$$

$$r_{eq1} = r_L + r_{M\,P} / 2, \quad (8)$$

$$r_{eq2} = r_L + r_{M\,P} + r_P / 2 + \\ +2r_S / (2n)^2 + 2r_{M\,S} / (2n)^2, \quad (9)$$

$$N_e = n, \quad (10)$$

$$r_{eq1} = r_L + r_{M\,P}, \quad (11)$$

$$r_{eq2} = r_L + 4r_{M\,P} + 2r_P + \\ +2r_S / n^2 + 2r_{M\,S} / n^2. \quad (12)$$

Based on the conduction states shown in Fig.10 and Fig. 11, a new model can be obtained for normal and extended operating voltage mode. The state equation of the system is obtained as shown in (13)

$$d / dt \begin{pmatrix} i_L(t) \\ v_{C\,A}(t) \\ v_{C\,B}(t) \end{pmatrix} = A \cdot \begin{pmatrix} i_L(t) \\ v_{C\,A}(t) \\ v_{C\,B}(t) \end{pmatrix} + B \cdot \begin{pmatrix} V_g \\ V_{OC\,Bat} \end{pmatrix}. \quad (13)$$

The averaged value of the input and state matrixes is obtained by averaging (5), (6), (16) and (17) over the inductor period as shown in (14) and (15):

$$A = A_1 \cdot d + A_2 \cdot (1-d), \quad (14)$$

$$B = B_1 \cdot d + B_2 \cdot (1-d). \quad (15)$$

$$A_1 = \begin{pmatrix} -\frac{1}{L}\left(r_{eq1} + \frac{r_{esr_A} \cdot R_g}{R_G + r_{esr_A}} \right) & \frac{R_g}{L\left(R_g + r_{esr_A}\right)} & 0 \\ -\frac{R_g}{C_A\left(R_g + r_{esr_A}\right)} & -\frac{1}{C_A\left(R_g + r_{esr_{IN}}\right)} & 0 \\ 0 & 0 & -\frac{1}{C_B\left(R_{D_{Bat}} + r_{esr_B}\right)} \end{pmatrix}, \quad (16)$$

$$A_2 = \begin{pmatrix} -\frac{1}{L}\left(r_{eq2} + \frac{r_{esrB}\cdot R_{D_{Bat}}}{4N_e^2\left(R_{D_{Bat}} + r_{esrB}\right)} + \frac{r_{esr_A}\cdot R_g}{R_g + r_{esr_A}} \right) & \frac{R_g}{L\left(R_g + r_{esr_A}\right)} & -\frac{R_{D_{Bat}}}{L\left(R_{D_{Bat}} + r_{esrB}\right)} \\ -\frac{R_g}{C_A\cdot\left(R_g + r_{esr_A}\right)} & -\frac{1}{C_A\left(R_g + r_{esr_A}\right)} & 0 \\ \frac{R_{D_{Bat}}}{4\cdot C_B\cdot N_e^2\left(R_{D_{Bat}} + r_{esrB}\right)} & 0 & -\frac{1}{C_B\left(R_{D_{Bat}} + r_{esrB}\right)} \end{pmatrix}. \quad (17)$$

In order to reduce the current stress during the transition between normal and extended voltage range mode, the converter MOSFETs' duty cycle is computed prior to the transition by calculating the steady-state solution from (13) as shown in (18)

$$D = 2[1-(I_L\cdot\left(R_g + R_{D_{Bat}} / N_e{}^2 + r_{eq2}\right)+ +V_{OC\,Bat} / N_e - V_g) / (I_L\cdot(R_{D_{Bat}} / N_e{}^2 + +r_{eq2} - r_{eq1}) + V_{OC\,Bat} / N_e)]. \quad (18)$$

Equation (18) is simplfied by taking into account that the input and ouput capacitors do not affect the converter duty cycle-to-inductor current steady-state solution.

Nevertheless, a calculation based on this equation presents a very high computational demand because the battery dynamic resistance is strongly dependent on the battery state of charge (SOC). On the other hand, if the input and output voltages of the converter (V_A,V_B) are measured during operation, expression of (18) can be reduced to (19)

$$D = 2[1-\left(I_L\cdot r_{eq2} + V_B / N_e - V_A\right) / / \left(I_L\cdot\left(r_{eq2} - r_{eq1}\right) + V_B / N_e\right). \quad (19)$$

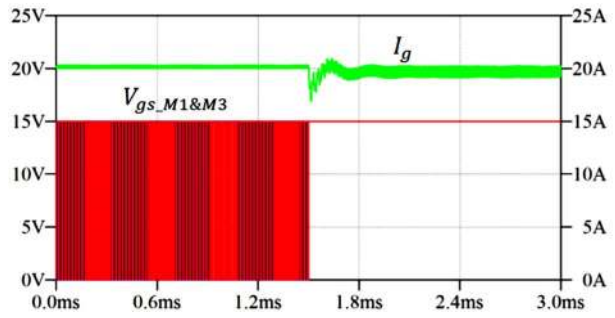

Fig. 14. Simulated transition between operating modes with pre-calculated steady-state duty cycle. Converter input current I_g (green), M1 and M3 gate signal (red and blue).

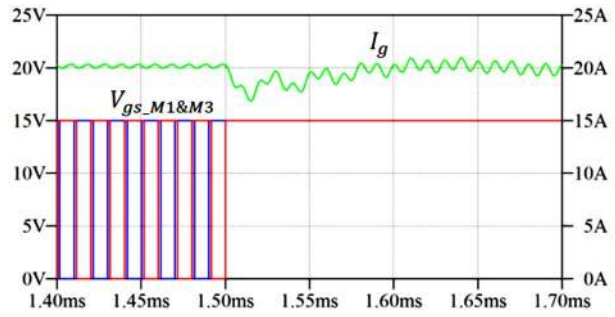

Fig. 15. Detailed enlarged area of the transition. Converter input current I_g (green), M1 and M3 gate signal (red and blue).

Figure 14 and Fig. 15 show an LTSpice simulation of a transition event where the controller has been set to produce the pre-calculated duty cycle before the transition event between normal and extended operating modes.

V. Experimental Results

A digitally controlled PPIBC has been used to experimentally verify the operation of the converter in extended mode. Each of the converter magnetic components is implemented with four planar ELP64/10/50 parts in N87 material. The primary and secondary switches are 150V N-channel MOSFETs IRFP4568. The converter control board is based on a 32 bit fixed point digital signal processor (DSP) TMS320F28035. The gate signals in one of the paralleled primary stages have been modified by inserting some control logic circuitry to produce the desired waveforms under the extended operation mode. The implemented prototype and the gate drive circuitry are shown in Fig. 16 and Fig. 17 respectively. Figure 18 shows the prototype operating waveforms during normal operation mode.

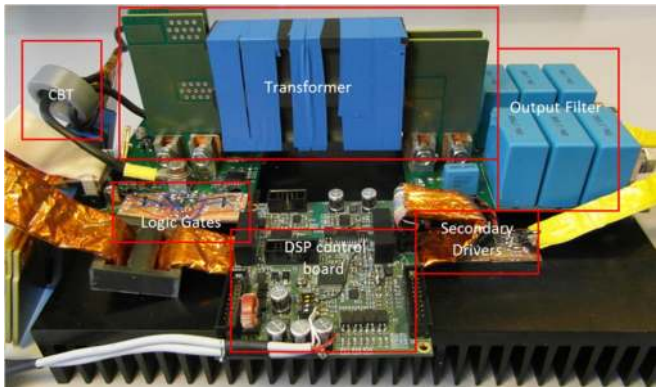

Fig. 16. PPIBC experimental prototype.

Figure 19 presents the converter operating waveforms during extended operating mode. The inductor current shows a change in the slope. During this mode, the magnetizing inductance of the current balancing transformer appears in series with the input inductor. However, the current balancing transformer saturates during this operation mode causing the change in the inductor current slope. The converter's efficiency in normal and extended operation modes can be observed in Fig. 20. The efficiency in the extended mode is measured at half the output voltage in normal mode. As it can be seen, the efficiency in extended operation mode decreases compared to the normal mode.

This is due to the higher current stress in the secondary side, the increased conduction losses in the primary side and

the increased transformer leakage inductance during the extended mode.

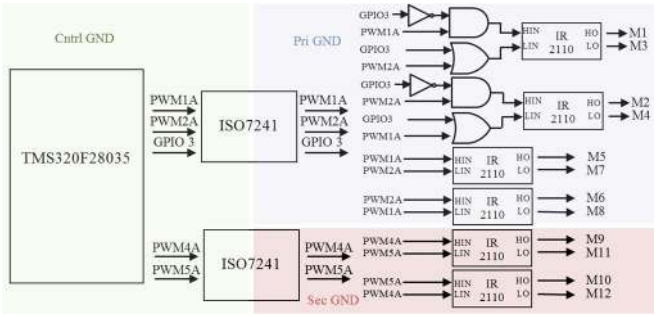

Fig. 17. Gate drive circuitry.

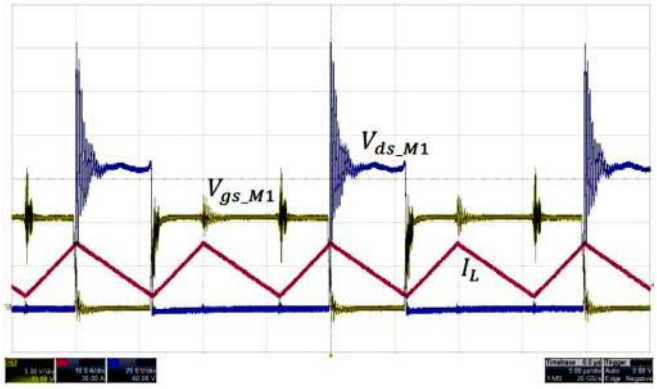

Fig. 18. Converter operating waveform during normal operation mode. M1 gate signal (brown, 5 V/div), M1 drain to source voltage signal (blue, 20 V/div) time scale 5 µs/div.

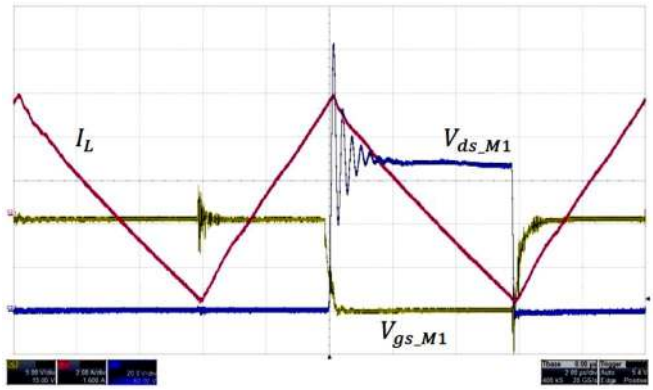

Fig. 19. Converter operating waveform during extended operation mode. M1 gate signal (brown, 5 V/div), M1 drain to source voltage signal (blue, 20 V/div) time scale 2 µs/div.

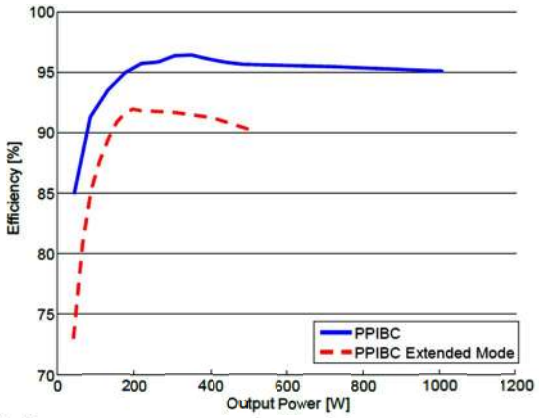

Fig. 20. Converter efficiency comparison between operating modes (blue, normal mode $V_{in} = 40\,V$ and $V_o = 45\,V$ and red $V_{in} = 40\,V$ and $V_o = 22.5\,V$).

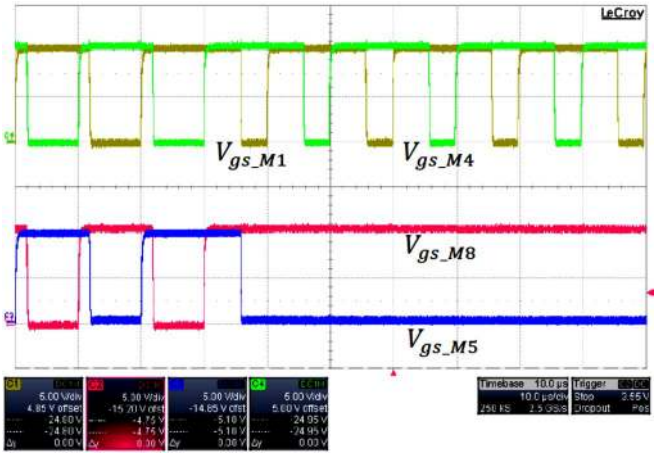

Fig. 21. Gate waveforms during normal to extended operating mode transition (b). M1 and M4 gate signals (brown and green, 5 V/div), M5 and M8 gate signals (blue and red, 5 V/div) time scale 100 µs/div.

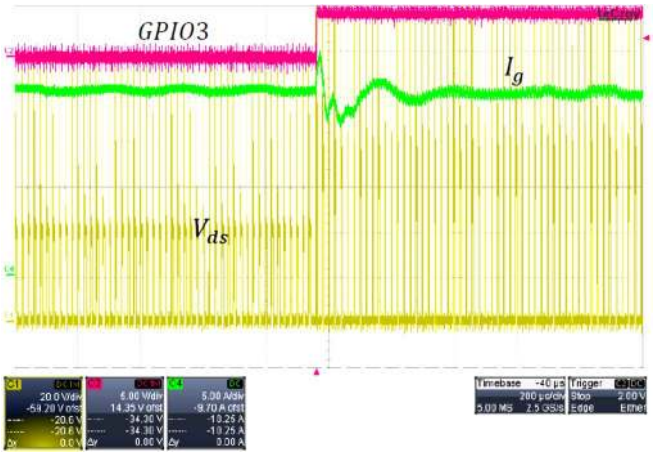

Fig. 22. Transition between operating modes with pre-calculated steady-state duty cycle. Time scale: 200 µs/div. Source output current I_g (green, 5 A/div), primary MOSFET drain to source voltage (brown, 20 V/div) and short circuit control signal GPIO3 (red, 5 V/div).

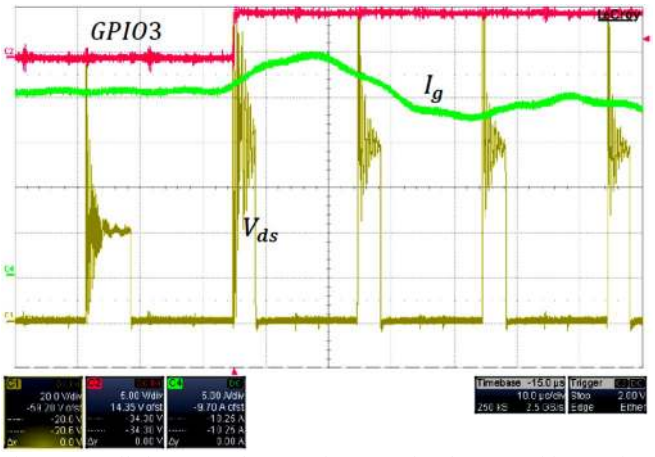

Fig. 23. Detailed zoomed waveforms of the transition Time scale:10 µs/div). Source output current I_g (green, 5 A/div), primary MOSFET drain to source voltage (brown, 20 V/div) and short circuit control signal GPIO3 (red, 5 V/div).

Figure 21–Fig. 23 show a transition event from normal to extended operating mode with pre-calculated duty cycle during converter closed loop operation for an inductor current level equal to 20 A. The change in duty cycle and voltage stress can be observed in one of the primary MOSFETs drain to source voltage waveform. It can be noticed that during extended operation mode, the voltage

ringing at the MOSFET off state increases with respect to the normal operation mode due to the effect of the leakage inductance of the short circuited transformer.

VI. Conclusions

In applications requiring wide operating voltage ranges, extreme duty cycles and extreme turn ratios for transformers have to be selected for covering the converter specifications, which will affect converter efficiency. Therefore, optimizing converter design for the most probable operating conditions and still covering all the possible operating points is desired. In order to do this, a new method for extending the operating voltage range has been proposed for PPIBC. The effective converter voltage conversion ratio is changed by deactivating one of the transformers through short-circuiting its primary windings. This new operation mode has been tested in a series of simulations and experiments where it has been observed that the transition between normal and extended operating modes is a disturbance to the converter due to the change in steady-state operating conditions. However, a smooth transition can be obtained if the steady-state duty cycle is pre-calculated based on an accurate model of the converter. This is an alternative solution to the auxiliary flyback winding in PPIBC.

References

[1] M. Nymand, M. A. E. Andersen, "New primary-parallel boost converter for high-power high-gain applications" in *Proc. IEEE Applied Power Electronics Conference*, Washington, DC, 2009, pp. 35–39.

[2] M. Nymand, M. A. E. Andersen, "A new approach to high efficiency in isolated boost converters for high-power low-voltage fuel cell applications", in *Proc. Power Electronics and Motion Control Conference*, Poznan, Poland, 2008, pp. 127–131.

[3] L. Zhu, K. Wang, F. C. Lee, J.-S. Lai, "New start-up schemes for isolated full-bridge boost converters", in *IEEE Trans. Power Electron*., vol. 18, pp. 946–951, 2003. [Online]. Available: http://dx.doi.org/10.1109/TPEL.2003.813758

[4] G. Sen, S. M. Dehghan, O. C. Thomsen, M. A. E. Andersen, "Comparison of current balancing configurations for primary parallel isolated boost converter", in *Proc. Electrical Machines and Power Electronics and 2011 Electromotion Joint Conf.*, Istanbul, 2011, pp. 449–454.

[5] S. N. Motapon, O. Tremblay, L.-A. Dessaint, "A generic fuel cell model for the simulation of fuel cell power systems", in *Proc. Power and Energy Society General Meeting*, Calgary, 2009, pp. 1–8.

[6] A. Al-Haj Hussein, "An overview of generic battery models", in *Proc. Power and Energy Society General Meeting*, San Diego, CA, 2011, pp. 1–6.

[7] K. Lindberg-Poulsen, Z. Ouyang, G. Sen, M. A. E. Andersen, "A new method for start-up of isolated boost converters using magnetic- and winding-integration" in *Proc. IEEE Applied Power Electronics Conference*, Orlando, Florida, 2012, pp. 340–345.

[8] M. C. Mira, J. C. Hernandez, G. Sen, O. C. Thomsen, M. A. E. Andersen, "Modeling and control of primary parallel isolated boost converter", in *Proc. 38th Annual Conf. IEEE Industrial Electronics Society*, Montreal, 2012, pp. 555–560.

[9] J. C. Hernandez, M. C. Mira, G. Sen, O. C. Thomsen, M. A. E. Andersen, "Primary parallel isolated boost converter with bidirectional operation", in *Proc. Vehicle Power and Propulsion Conf.*, Seoul, 2012, pp. 794–799.

[10] J. C. Hernandez, M. C. Mira, G. Sen, O. C. Thomsen, M. A. E. Andersen, "Primary parallel isolated boost converter with extended operating voltage range" in *Proc. The European Workshop on Renewable Energy Systems*, Antalya, 2012.